Interfacial Symmetry-Breaking Effects in the Quantum Paraelectric SrTiO₃

Hang-Bo Zhang[†] and Marin Alexe[*]

Department of Physics, University of Warwick, Coventry CV4 7AL, United Kingdom

Oxides lacking a center of symmetry are highly desired, as they usually have fascinating physical properties. However, there are limited numbers of noncentrosymmetric media in nature and most of them do not have multiple functionalities integrated. Here, using the bulk photovoltaic effect as the probing technique, we demonstrate that, at interfaces with a wide range of oxides, strontium titanate (SrTiO₃) is polar, i.e., with broken inversion symmetry in the quantum paraelectric phase. Studies comprising conductivity and the bulk photovoltaic effect on LaAlO₃/SrTiO₃ thin films further show that excessive electronic band bending screens the induced polarity, revealing that appropriate band bending at the interface is the key parameter to control symmetry breaking. Inheriting high carrier mobility from SrTiO₃, the polar interface under illumination at low temperatures is conductive or metallic, permitting multifunctionality coupling between the oxides and SrTiO₃. Our studies show that significant photovoltaic effects can be generated at the polar interfaces, especially in the quantum-paraelectric phase of SrTiO₃, thus giving practical design strategies for multifunctional devices.

I. INTRODUCTION

SrTiO₃ (STO) and its heterostructures with dissimilar materials are proven to show fascinating physical functionalities, especially in the low-temperature regime. The ultrahigh dielectric constant [1,2], two-dimensional electron gas (2DEG) [3,4], and superconductivity [5,6] are only a few emerging properties usually associated with either high carrier mobility [7] or the quantum paraelectric phase [8,9] of STO. The quantum paraelectricity, where quantum fluctuations between degenerate lower-symmetry configurations suppress ferroelectric ordering [2], can be further induced into a polar state by an external field [9] or chemical substitution [10,11], enriching the functionality of the system or even coupling ferroelectricity and ferromagnetism and superconductivity [12,13]. All these interesting properties make STO one of the most popular materials for oxide electronics [14].

As recently highlighted, band bending at a metal-oxide (Schottky) junction is inherently associated with a built-in electric field [15], which breaks the inversion symmetry at the interface. This is, in principle, not a characteristic of a metal-semiconductor interface. A built-in electric field commonly exists at the interface of any two dissimilar materials (e.g., metal-semiconductor, semiconductor-semiconductor) due to generic band bending needed to align the Fermi level across the interface [16,17]. For STO,

a polar interface might be easily induced at the quantum paraelectric phase regime.

We show here that many oxide-STO heterostructures have polar interfaces in the quantum paraelectric regime of STO, as detected by a bulk photovoltaic effect that exists only in noncentrosymmetric media. Furthermore, we demonstrate that the magnitude of the polarity of the interface can be tuned in the LaAlO₃-SrTiO₃ (LAO/STO) system by fabrication conditions. These properties along with the well-known high carrier mobility of STO could bring unexpected properties, such as metallic ferroelectricity [18].

II. EXPERIMENTS

A. Synthesis of SrTiO₃-based heterostructures

TiO₂-terminated (001)-oriented SrTiO₃ substrates are etched in buffered HF for 15 s and then annealed in air at 1200 °C for 2 h. LAO/STO thin films are grown by pulsed laser deposition (PLD) at 10^{-3}-mbar oxygen pressure. The laser energy density is 1 J/cm² and the repetition rate is 2 Hz. Samples LAO/STO 1, 2, 3, and 4 are grown at 600, 650, 700, and 750 °C, respectively. The LAO thin-film thickness is, in all cases, about 10 nm. About 50-nm-thick Fe₂O₃ thin films are deposited on STO by PLD at 10^{-5} mbar and 600 °C, with a laser fluence of 0.5 J/cm² and a repetition rate of 5 Hz. 40-nm Au and 20-nm Al are evaporated on the surface of SrTiO₃ to fabricate Au/STO and Al/STO, respectively.

*m.alexe@warwick.ac.uk
†hangbozhang@outlook.com

B. Electrical measurements

The homemade optical physical property measurement system (PPMS) insert is used for 10–300 K temperature-dependent measurements. A polarized 405 nm laser (40-mW nominal power, Thorlabs, DL5146-101S) is used to generate linearly polarized light. The light polarization direction is rotated at a rate of 2 °/s using a half-wave plate (HWP; Thorlabs, model AHWP05M-340). A high-impedance electrometer (Keithley 6517B) is used to collect the time-dependent photocurrent, i.e., wave-plate angle-dependent photocurrent. An AixACCT TF3000 ferroelectric workstation is employed to study the ferroelectric polarization switching behavior in our work. For each electrical measurement, we stabilize the system for sufficient time until the current-drift effect or light-induced heat vanishes. (See details in Fig. 6 in Appendix C.)

III. RESULTS

A. Characterization of general symmetry breaking

Several oxide layers, as well as noble metals (Au), are deposited on the (100) surface of (100)-oriented STO single crystals to induce band bending at the interface. The light-polarization-dependent bulk photovoltaic (BPV) effect is used to probe interface symmetry breaking underneath the capping layer [19], as the BPV effect exists only in noncentrosymmetric media. If the innate centrosymmetry of the crystal is lifted and becomes polar, a BPV current is generated by light penetrating the capping layer

[20]. As a proof-of-concept experiment, the BPV current is first measured on a metal-semiconductor junction (Schottky) fabricated by depositing a high-work-function metal that usually generates large band bending within STO. As expected, the Au/STO system shows, at room temperature, a textbook linear BPV effect, indicating symmetry breaking at the interface by simply contacting gold with the centrosymmetric STO crystal [15,20]. Figure 1(b) shows the variation of photovoltaic (PV) current with respect to the relative angle between light polarization and crystallographic direction of the PV current, which is the fingerprint of the linear BPV (LBPV) effect. This angle is set using a HWP; therefore, hereafter it is denoted as the HWP angle, θ. According to phenomenological theory [20,21], the LBPV current as a function of the HWP angle is expressed as

$$J^{\mathrm{HWP}} = J_L \sin(4(\theta + \theta^{\mathrm{off}})) + J_L^{\mathrm{off}}, \qquad (1)$$

where J_L is the amplitude of the LBPV current, θ^{off} is the LBPV angle offset, and J_L^{off} is the LBPV current offset that is independent of the HWP angle. By least-squares fitting of the HWP angle-dependent photocurrent [as in Fig. 1(b)], we obtain the amplitude of the LBPV current and use it to characterize the LBPV effect.

To characterize the BPV effect in the quantum paraelectric regime of STO, one needs to lower the temperature under a characteristic transition temperature of about 37 K and simultaneously measure the PV current. For this purpose, a PPMS with a homemade optical insert,
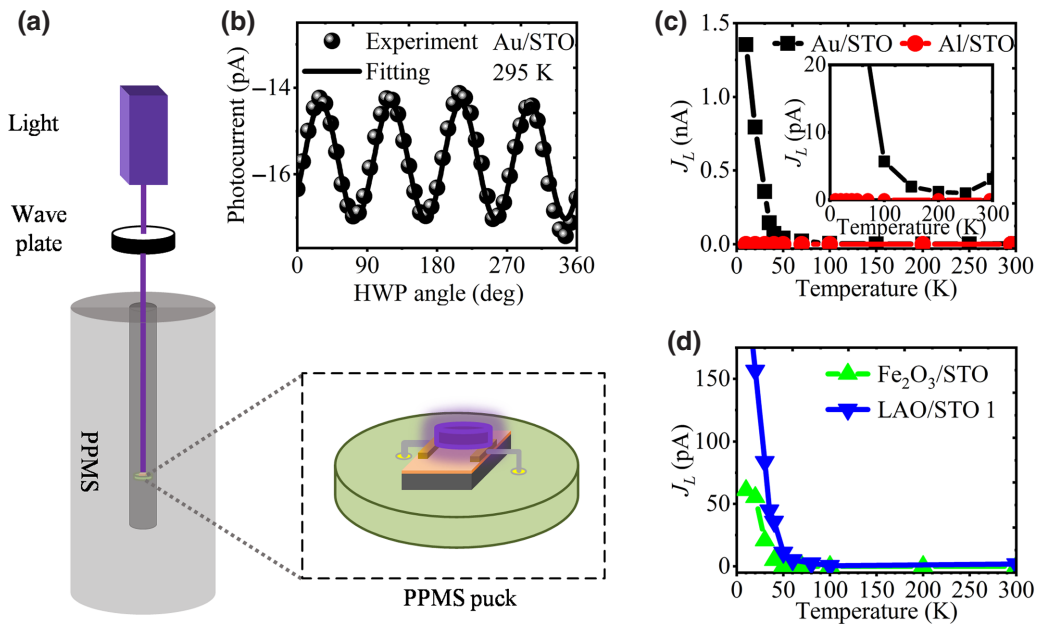

FIG. 1. Detection of general symmetry breaking of STO-based heterostructures via linear BPV effect. (a) Schematic of the homemade optical PPMS. (b) HWP angle-dependent photocurrent of simple Au/STO junction at room temperature. (c) Temperature-dependent LBPV current amplitudes of Schottky Au/STO contact and quasi-ohmic Al/STO contact. Inset is an enlarged view of LBPV current amplitudes. (d) Temperature-dependent LBPV current amplitudes of Fe_2O_3/STO and LAO/STO 1.
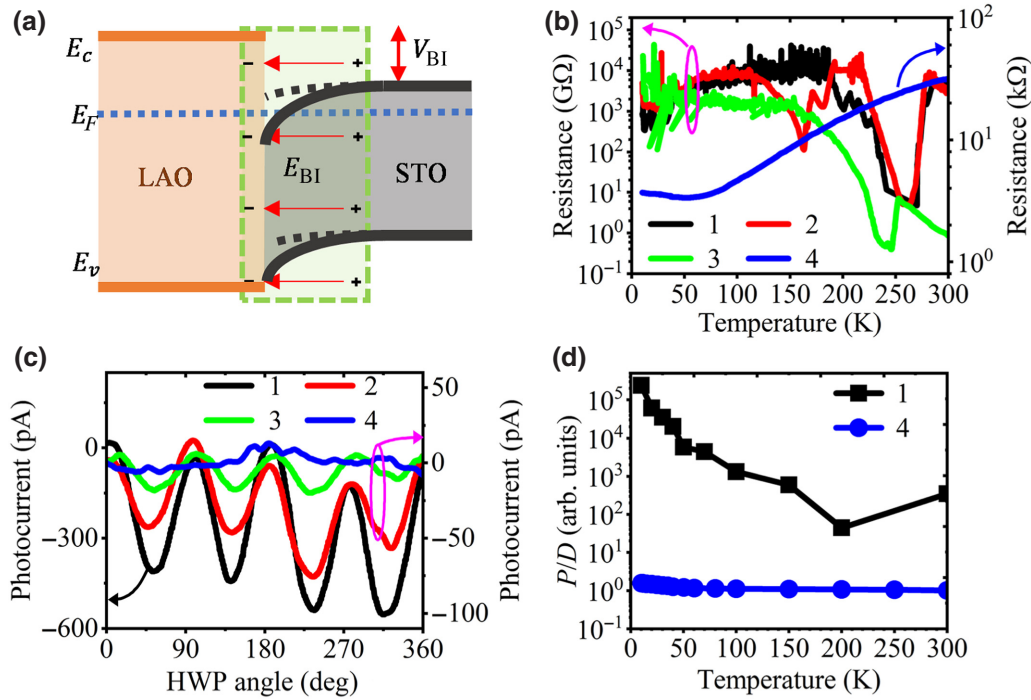
FIG. 2. LBPV effect and conductivity characterization of LAO/STO thin films grown at different temperatures. Samples 1, 2, 3, and 4 are grown at 600, 650, 700, and 750 °C, respectively. (a) Illustration of band bending at the interface of LAO/STO. V_{BI} is the built-in voltage and E_{BI} is the built-in electric field. E_c, E_v, and E_F are the conduction band, valence band, and Fermi level, respectively. (b) Temperature-dependent dark resistance of LAO/STO grown at different temperatures. Below 200 K, dark-current measurements of LAO/STO 1, 2, and 3 are limited by current sensitivity, as the dark resistance is very high. (c) HWP angle-dependent linear photovoltaic currents at 10 K of LAO/STO grown at different temperatures. (d) Ratio of photoconductivity to dark conductivity (P/D) of LAO/STO 1 and 4 as a function of temperature.

schematically shown in Fig. 1(a), is used to characterize the optoelectrical properties from room temperature to 10 K. The linearly polarized light modulated by a half-wave plate allows us to analyze the linear BPV current of the investigated samples [22].

As we decrease the temperature of Au-STO, a remarkable increase of the photocurrent by about 3 orders of magnitude is observed below about 40 K [Fig. 1(c)]. To exclude this LBPV response from the contribution of pristine STO bulk or surface, we conduct similar experiments on STO with quasi-ohmic contacts, i.e., aluminum. As expected, due to the low work function, Al does not provide sufficient band bending at the Al/STO interface. Consequently, Al/STO does not show a BPV effect over the entire temperature range [see Figs. 1(c) and 4(b) in Appendix A]. These results are consistent with a previous report that the metal-oxide Schottky junction can induce a polar structure at the interface, while the ohmic contact cannot [15].

To investigate whether symmetry breaking also exists in oxide-STO interfaces, we first study the LBPV effect in a Fe_2O_3/STO thin film. Neither of these materials should, in principle, show the BPV effect at any temperature. While this is true for high temperatures, by lowering the

temperature under 40 K, a considerable LBPV response is observed [Fig. 1(d)]. Since both STO and Fe_2O_3 are centrosymmetric and normally do not show the BPV effect, their interface must be the origin of this giant LBPV response. We assume that this might be a generic effect, in which bringing STO into the quantum paraelectric state lowers its temperature below the transition temperature, which is an important feature. We further investigate the LBPV effect in LAO/STO heterostructures, as examples of iconic STO-based interfaces that were extensively investigated in the recent past [3,5].

Knowing that the electronic characteristics of this system are very sensitive to the growth conditions [23,24], we fabricate heterostructures by depositing LAO thin films on STO under the specific condition in which the 2DEG state is not yet formed, i.e., LAO/STO 1 thin film in our experiment [Fig. 2(b)]. Similarly to the Au/STO system, LAO/STO 1 has a weak BPV response at room temperature, which increases by several orders of magnitude below 40 K, as shown in Figs. 1(d) and 4(d) in Appendix A.

The onset temperature of the massive LBPV response is about 40 K, which is close to the temperature of the emergence of the quantum paraelectric phase (37 K) in STO [9]. However, the nonpolar quantum paraelectric state is
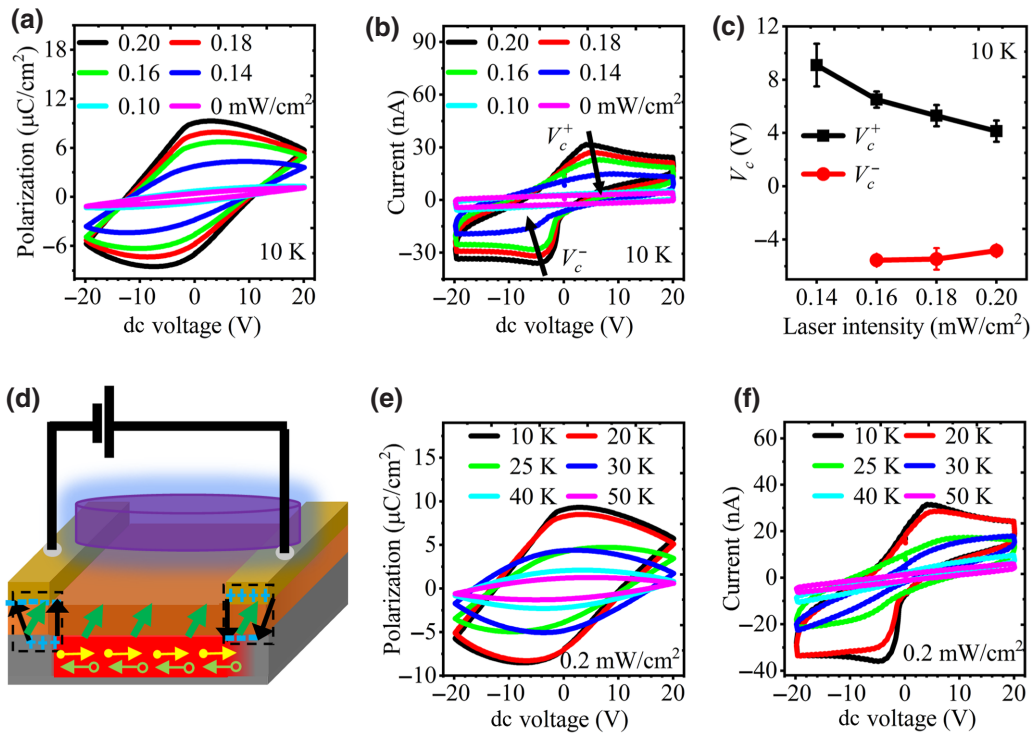
FIG. 3.   Ferroelectric *P-V* hysteresis loop of BFO/STO thin film under illumination. Laser-intensity-dependent (a) *P-V* loops, (b) *I-V* curves, and (c) coercive voltage at 10 K. (d) Schematic illustration of *P-V* loop measurements. Yellow solid dots and light-green open circles represent electrons and holes, respectively; corresponding arrows indicate the movement directions upon application of a dc voltage. Black arrows indicate the electric field across the thin film. Green arrows indicate ferroelectric polarization of the thin film. Black dashed square boxes indicate polarization in operation. Temperature-dependent (e) *P-V* loops and (f) *I-V* curves are measured under illumination at a laser intensity of 0.2 mW/cm^2.

centrosymmetric and should, in principle, not show any BPV effect. Experimental evidence points us to the fact that this quantum paraelectric phase is in an ordered polar phase at the interface. It is well known that, at the interface of any heterostructures based on two dissimilar materials, a built-in voltage, V_{BI}, exists, as a result of band alignment to maintain the Fermi energy level flat across the interface [17] [e.g., LAO/STO system shown in Fig. 2(a)]. This band bending results in a built-in electric field, E_{BI}, normal to the interface and forms a polar interface [15].

B. The tunable polarity of the interface of the LAO/STO system

Next, we explore whether this polarity of the interface can be tuned or controlled through the fabrication process. Therefore, we focus on the well-studied LAO/STO heterostructures. It is known that band bending in STO induces either a conductive or an insulating interface, depending upon the position of the Fermi level with respect to the conduction band [17,25,26]. For example, if the conduction band at the interface is bent well below the Fermi level, a large density of available states becomes available, and the carriers may become mobile at the interface

[Fig. 2(a)]. It is known that oxygen vacancies are playing a key role in providing free electrons and tuning the interface conductivity [27,28]. To clarify the effect of electronic reconstruction on the polarity of the interface, as they are under the same influence of interfacial band bending, we investigate the BPV effect and conductivity of a series of LAO/STO thin films with different interface doping densities. The latter is tuned by simply controlling the growth temperature of LAO thin films on STO substrate [29,30] (see Sec. II).

The temperature-dependent dark-resistance measurements [Fig. 2(b)] confirm that the growth temperature can effectively tune the interface carrier density. Only LAO/STO grown at 750 °C (LAO/STO 4) shows typical 2DEG temperature dependence of resistance, as previously reported [31]. Samples grown at lower temperatures show much higher resistance and non-2DEG-like temperature dependence [Fig. 2(b)]. Then, we study the relationship between the LBPV currents and growth temperature. Interestingly, the LBPV response is opposite to the resistance behavior in the LAO/STO system. The LBPV current of the LAO/STO thin film grown at the lowest temperature, 600 °C (LAO/STO 1), is at least 1 order of magnitude higher than that measured on samples grown at higher

temperatures. The presence of the LBPV effect indicates that symmetry breaking at the LAO/STO interface and, implicitly, the polar nature of the interface, is stronger in LAO/STO 1 compared to all other samples. Noticeably, LAO/STO grown at 750 °C (LAO/STO 4), showing 2DEG behavior, does not exhibit any LBPV response.

The disjunction between the 2DEG and LBPV effects in LAO/STO reveals an apparent screeninglike effect. In the 2DEG state, the thermally activated carrier density at the interface is so high that it either leaves no more available electronic states for photoexcited carriers or it exceeds the density of photogenerated carriers [32]. The ratio of photoconductivity to dark conductivity (P/D) of the LAO/STO thin films [Fig. 2(d)] supports this scenario. The conductivity of STO in the 2DEG state (LAO/STO 4) is barely changed under illumination. However, for the insulating sample, LAO/STO 1, the photoinduced carriers rule the carrier density of the system, remarkably enhancing the conductivity.

C. Photocontrolled conductive interface

After showing the symmetry-breaking nature of the oxide-STO system, we now investigate the conductivity of the interface, as it is well known that the carrier mobility of SrTiO$_3$ is very high at low temperatures. The interface of oxide-SrTiO$_3$ should, in principle, inherit this property and exhibit high conductivity or even metallic behavior. To verify this, we conduct polarization versus electric field measurements for an epitaxial BiFeO$_3$ (BFO) thin film deposited on STO (BFO/STO). If the interface is highly conductive, it will behave like a bottom metal underneath the oxide, allowing BFO polarization to switch upon an external bias voltage being applied to the top electrodes [see Fig. 3(d)].

Ferroelectric hysteresis versus electric field (P-V) loops and current versus electric field (I-V) measurements of BFO/STO monodomain thin films are recorded using an AixACCT TF3000 ferroelectric workstation under simultaneous illumination with 405-nm monochromatic light. The polarization [Fig. 3(a)] and current [Fig. 3(b)] versus applied voltage at 10 K reveal either dielectric or ferroelectric behavior, depending on the illumination conditions. Classic dielectric behavior is seen in the dark and under low-intensity illumination. Clear current peaks associated with polarization switching are seen under high-laser-intensity illumination, indicating partial switching of ferroelectric polarization at a coercive voltage, V_c, of about 4–6 V. The light-intensity dependence of V_c, i.e., the coercive voltage decreases with increasing laser intensity [Fig. 3(c)], provides evidence of the facile control of ferroelectricity via in-plane geometric electrodes.

We notice that ferroelectric polarization ($\sim$8 μC/cm^2) at 10 K is about 10% of the expected value of BFO thin films. This is probably due to partial polarization switching

of BFO [Fig. 3(d)]. Only a limited amount of photocarriers may diffuse underneath the top metal electrode to screen polarization while switching. As the temperature approaches 40 K, the electron mobility of STO dramatically drops and switching cannot be performed [Figs. 3(e) and 3(f)].

IV. CONCLUSION

The aforementioned experiments and analysis show that interfaces of STO with different oxides, such as Fe$_2$O$_3$ and LAO, are generating a built-in electric field and polar state in STO, including in the quantum paraelectric phase. The above effects might be a more general property of the STO interface with classical oxides, where the internal electrostatic potential is about a few hundred meV, corresponding to an electric field beneath the STO surface of about 1 mV/nm [33,34]. Such a high interface built-in field might be able to induce a quantum ferroelectric state, according to the electric field–temperature phase diagram [35] (see Fig. 5 in Appendix B).

In contrast to the 2DEG interface, which undergoes significant electronic reconstruction, the insulating interface with fewer initially trapped carriers during sample growth is more prone to a polar state. Nevertheless, even in the insulating state, the oxide-STO interface can still be conductive if sufficient free electrons, such as photocarriers generated under illumination, are provided [36]. Therefore, the photoconductive interface bridges the capping layer and STO substrate and largely extends the multifunctional degrees of freedom, e.g., spin-charge conversion, as recently highlighted [37]. Our work shows not only that a bulk photovoltaic effect can be used to detect the symmetry breaking of media, but also reveals that STO-based heterostructures are promising for designing multifunctional devices.

APPENDIX A: LINEAR BULK PHOTOVOLTAIC CURRENT MEASUREMENTS

Photocurrents as a function of the HWP angle are individually measured at different temperatures to determine the polarity of the structure. Linear bulk photovoltaic currents for Au/STO, Al/STO, Fe$_2$O$_3$/STO, and LAO/STO are given in Fig. 4. Clearly, Au/STO and LAO/STO 1, at
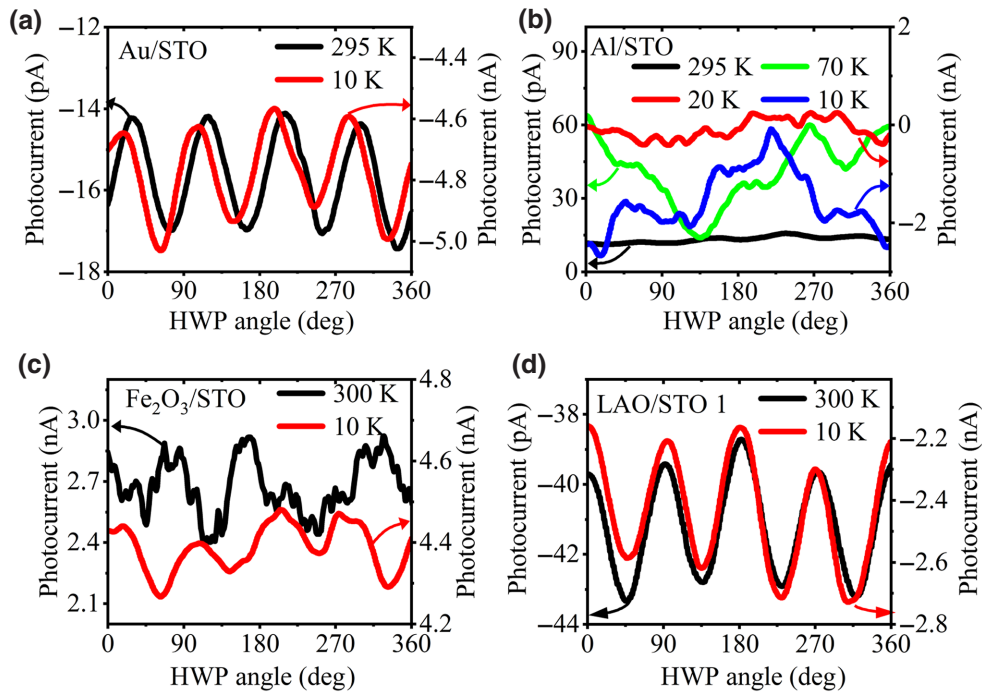
FIG. 4. HWP angle-dependent photocurrents of (a) Au/STO, (b) Al/STO, (c) Fe_2O_3/STO, and (d) LAO/STO 1 at different temperatures.

both high and low temperatures, show a classical bulk photovoltaic effect. On the contrary, Al/STO does not show any bulk photovoltaic effect at both high and low temperatures. The Fe_2O_3/STO sample does not show a bulk photovoltaic effect at room temperature; however, it shows bulk-photovoltaic-effect behavior at 10 K.

APPENDIX B: ELECTRIC FIELD–TEMPERATURE PHASE DIAGRAM OF STO

To further understand why the bulk photovoltaic effect becomes stronger when the temperature is lowered in the quantum paraelectric phase of STO, we employ the phase diagram of STO, as shown in Fig. 5 [35]. As is known, when the temperature is decreased in the quantum paraelectric phase, STO approaches the virtual Curie temperature (below 0 K) [8,9]. This indicates that (a) an electrical field to induce a polar structure in STO is less needed; and (b) a fixed electrical field can induce stronger polarity. Although we cannot verify if this interface enters a ferroelectric state more than a polar state, the phase diagram still applies to our above analysis for a normal polar state.

APPENDIX C: PHOTOCURRENT VERSUS LASER-SPOT POSITION

To prove that the photocurrent is not due to the injection of carriers from electrodes but purely due to the

bulk photovoltaic effect generated by the polar LAO/STO interface, we conduct further experiments using an optical cryostat (Attodry800) at both room temperature, of which details are given below, and low temperature. A pair of Au-Al electrodes (spacing 500 μm) are fabricated on the top of the LAO/STO 1 sample, as shown in Fig. 6(a). The photocurrent is measured by shifting the laser spot (about 150-μm radius) from the Al electrode to the Au electrode. Due to the nature of the BPV effect, which allows the carriers to diffuse over a certain distance, the photocurrent can be collected, even if the laser spot is smaller than the distance between the electrodes [38]. The results in Figs. 6(b)
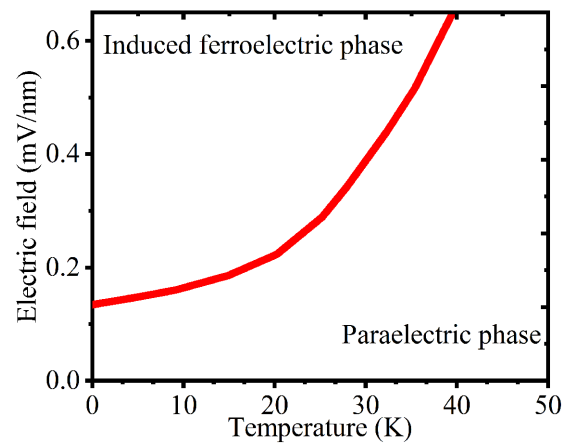

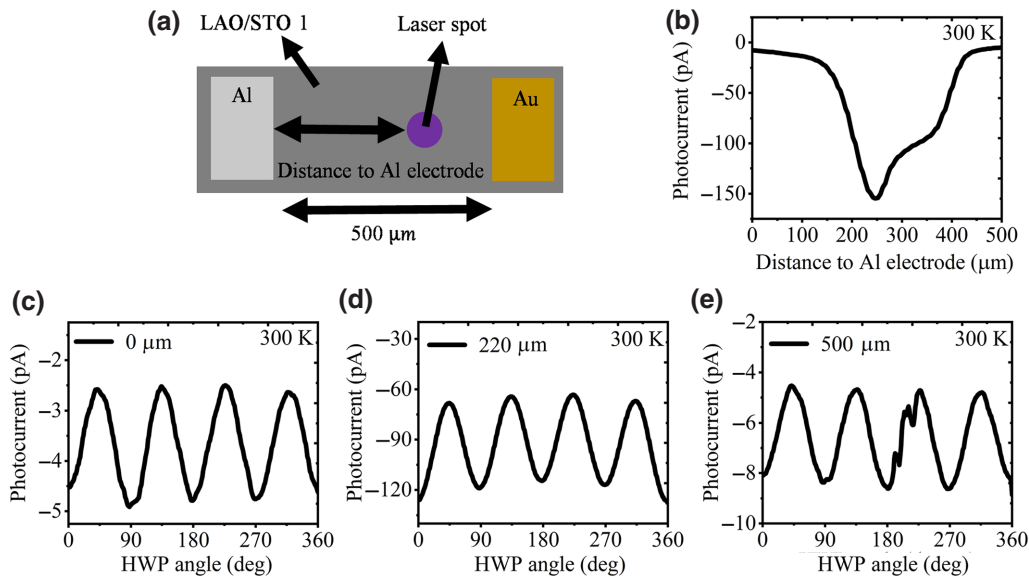FIG. 5. Electric field–temperature phase diagram of STO [35].

FIG. 6. Laser-spot-dependent photocurrent measurements. (a) Experimental setup. Al and Au electrode pair with a spacing of 500 μm is fabricated on the LAO/STO 1 sample. Laser spot is moved from the Al electrode to the Au electrode. (b) Photocurrent as a function of laser-spot position at 300 K. (c)–(e) Bulk photovoltaic currents measured at different laser-spot positions at 300 K. Glitch in (e) is due to the noise signal.

and 6(c)–6(e) clearly show that the photocurrent has a maximum value when the laser spot is in the middle of the electrode pair. It can be easily seen that if the illumination is on either the Au or Al electrodes, the photocurrent is negligible. This directly proves that the photocurrent is not due to the injection of the electrode but due to a proper internal photoelectric effect within the LAO/STO region. It is worth noting that the photocurrent flow is due to the bulk photovoltaic effect, which is anisotropic due to the symmetry properties of crystals or the structures (determined by the BPV tensor [19]). Therefore, the measured current in our experiments represents the in-plane component of the three-dimensional BPV current.

[1] E. Sawaguchi and A. Kikuchi, Dielectric constant of strontium titanate at low temperatures, J. Phys. Soc. Jpn. **17**, 1666 (1962).

[2] K. A. Müller and H. Burkard, SrTiO$_3$: An intrinsic quantum paraelectric below 4 K, Phys. Rev. B **19**, 3593 (1979).

[3] A. Ohtomo and H. Y. Hwang, A high-mobility electron gas at the LaAlO$_3$/SrTiO$_3$ heterointerface, Nature **427**, 423 (2004).

[4] S. Thiel, G. Hammerl, A. Schmehl, C. W. Schneider, and J. Mannhart, Tunable quasi-two-dimensional electron gases in oxide heterostructures, Science **313**, 1942 (2006).

[5] J. A. Bert, B. Kalisky, C. Bell, M. Kim, Y. Hikita, H. Y. Hwang, and K. A. Moler, Direct imaging of the coexistence of ferromagnetism and superconductivity at the LaAlO$_3$/SrTiO$_3$ interface, Nat. Phys. **7**, 767 (2011).

[6] N. Reyren, S. Thiel, A. D. Caviglia, L. F. Kourkoutis, G. Hammerl, C. Richter, C. W. Schneider, T. Kopp, A. S. Ruetschi, D. Jaccard, *et al.*, Superconducting interfaces between insulating oxides, Science **317**, 1196 (2007).

[7] O. Tufte and P. Chapman, Electron mobility in semiconducting strontium titanate, Phys. Rev. **155**, 796 (1967).

[8] K. A. Muller, W. Berlinger, and E. Tosatti, Indication for a novel phase in the quantum paraelectric regime of SrTiO$_3$, Z. Phys. B **84**, 277 (1991).

[9] J. Hemberger, M. Nicklas, R. Viana, P. Lunkenheimer, A. Loidl, and R. Bohmer, Quantum paraelectric and induced ferroelectric states in SrTiO$_3$, J. Phys. Condes. Matter **8**, 4673 (1996).

[10] M. Itoh, R. Wang, Y. Inaguma, T. Yamaguchi, Y. J. Shan, and T. Nakamura, Ferroelectricity Induced by Oxygen Isotope Exchange in Strontium Titanate Perovskite, Phys. Rev. Lett. **82**, 3540 (1999).

[11] J. G. Bednorz and K. A. Muller, Sr$_{1-x}$Ca$_x$TiO$_3$: An *XY* Quantum Ferroelectric with Transition to Randomness, Phys. Rev. Lett. **52**, 2289 (1984).

[12] C. W. Rischau, X. Lin, C. P. Grams, D. Finck, S. Harms, J. Engelmayer, T. Lorenz, Y. Gallais, B. Fauque, J. Hemberger, *et al.*, A ferroelectric quantum phase transition inside the superconducting dome of Sr$_{1-x}$Ca$_x$TiO$_3$-delta, Nat. Phys. **13**, 643 (2017).

[13] L. Li, C. Richter, J. Mannhart, and R. C. Ashoori, Coexistence of magnetic order and two-dimensional superconductivity at LaAlO$_3$/SrTiO$_3$ interfaces, Nat. Phys. **7**, 762 (2011).

[14] H. Y. Hwang, Y. Iwasa, M. Kawasaki, B. Keimer, N. Nagaosa, and Y. Tokura, Emergent phenomena at oxide interfaces, Nat. Mater. **11**, 103 (2012).

[15] M. M. Yang, Z. D. Luo, Z. Mi, J. J. Zhao, E. S. Pei, and M. Alexe, Piezoelectric and pyroelectric effects induced by interface polar symmetry, Nature **584**, 377 (2020).

[16] D. H. Choe, D. West, and S. B. Zhang, Band Alignment and the Built-In Potential of Solids, Phys. Rev. Lett. **121**, 196802 (2018).

[17] A. Klein, Energy band alignment at interfaces of semiconducting oxides: A review of experimental determination using photoelectron spectroscopy and comparison with theoretical predictions by the electron affinity rule, charge neutrality levels, and the common anion rule, Thin Solid Films **520**, 3721 (2012).

[18] Y. G. Shi, Y. F. Guo, X. Wang, A. J. Princep, D. Khalyavin, P. Manuel, Y. Michiue, A. Sato, K. Tsuda, S. Yu, *et al.*, A ferroelectric-like structural transition in a metal, Nat. Mater. **12**, 1024 (2013).

[19] V. I. Belinicher and B. I. Sturman, The photogalvanic effect in media lacking a center of symmetry, Sov. Phys. Usp. **23**, 199 (1980).

[20] B. I. Sturman and V. M. Fridkin, *The Photovoltaic and Photorefractive Effects in Noncentrosymmetric Materials* (Gordon and Breach Science Publishers, Philadelphia, 1992).

[21] A. Bhatnagar, A. R. Chaudhuri, Y. H. Kim, D. Hesse, and M. Alexe, Role of domain walls in the abnormal photovoltaic effect in $BiFeO_3$, Nat. Commun. **4**, 8 (2013).

[22] D. S. Knoche, M. Steimecke, Y. Yun, L. Muhlenbein, and A. Bhatnagar, Anomalous circular bulk photovoltaic effect in $BiFeO_3$ thin films with stripe-domain pattern, Nat. Commun. **12**, 282 (2021).

[23] J. Mannhart and D. G. Schlom, Oxide interfaces-an opportunity for electronics, Science **327**, 1607 (2010).

[24] D. A. Dikin, M. Mehta, C. W. Bark, C. M. Folkman, C. B. Eom, and V. Chandrasekhar, Coexistence of Superconductivity and Ferromagnetism in Two Dimensions, Phys. Rev. Lett. **107**, 056802 (2011).

[25] S. W. Zeng, X. M. Yin, T. S. Herng, K. Han, Z. Huang, L. C. Zhang, C. J. Li, W. X. Zhou, D. Y. Wan, P. Yang, *et al.*, Oxygen Electromigration and Energy Band Reconstruction Induced by Electrolyte Field Effect at Oxide Interfaces, Phys. Rev. Lett. **121**, 146802 (2018).

[26] G. Berner, A. Muller, F. Pfaff, J. Walde, C. Richter, J. Mannhart, S. Thiess, A. Gloskovskii, W. Drube, M. Sing, *et al.*, Band alignment in $LaAlO_3/SrTiO_3$ oxide heterostructures inferred from hard x-ray photoelectron spectroscopy, Phys. Rev. B **88**, 115111 (2013).

[27] Z. C. Zhong, P. X. Xu, and P. J. Kelly, Polarity-induced oxygen vacancies at $LaAlO_3/SrTiO_3$ interfaces, Phys. Rev. B **82**, 165127 (2010).

[28] Y. Li, S. N. Phattalung, S. Limpijumnong, J. Kim, and J. Yu, Formation of oxygen vacancies and charge carriers induced in the *n*-type interface of a $LaAlO_3$ overlayer on $SrTiO_3(001)$, Phys. Rev. B **84**, 245307 (2011).

[29] A. Kalabukhov, R. Gunnarsson, J. Borjesson, E. Olsson, T. Claeson, and D. Winkler, Effect of oxygen vacancies in the $SrTiO_3$ substrate on the electrical properties of the $LaAlO_3/SrTiO_3$ interface, Phys. Rev. B **75**, 121404(R) (2007).

[30] A. Fete, C. Cancellieri, D. Li, D. Stornaiuolo, A. D. Caviglia, S. Gariglio, and J. M. Triscone, Growth-induced electron mobility enhancement at the $LaAlO_3/SrTiO_3$ interface, Appl. Phys. Lett. **106**, 051604 (2015).

[31] G. Herranz, M. Basletic, M. Bibes, C. Carretero, E. Tafra, E. Jacquet, K. Bouzehouane, C. Deranlot, A. Hamzic, J. M. Broto, *et al.*, High Mobility in $LaAlO_3/SrTiO_3$ Heterostructures: Origin, Dimensionality, and Perspectives, Phys. Rev. Lett. **98**, 216803 (2007).

[32] S. A. Chambers, M. H. Engelhard, V. Shutthanandan, Z. Zhu, T. C. Droubay, L. Qiao, P. V. Sushko, T. Feng, H. D. Lee, T. Gustafsson, *et al.*, Instability, intermixing and electronic structure at the epitaxial $LaAlO_3/SrTiO_3(001)$ heterojunction, Surf. Sci. Rep. **65**, 317 (2010).

[33] S. A. Chambers, L. Qiao, T. C. Droubay, T. C. Kaspar, B. W. Arey, and P. V. Sushko, Band Alignment, Built-In Potential, and the Absence of Conductivity at the $LaCrO_3/SrTiO_3(001)$ Heterojunction, Phys. Rev. Lett. **107**, 206802 (2011).

[34] P. Schutz, F. Pfaff, P. Scheiderer, Y. Z. Chen, N. Pryds, M. Gorgoi, M. Sing, and R. Claessen, Band bending and alignment at the spinel/perovskite gamma-$Al_2O_3/SrTiO_3$ heterointerface, Phys. Rev. B **91**, 165118 (2015).

[35] J. Hemberger, P. Lunkenheimer, R. Viana, R. Bohmer, and A. Loidl, Electric-field-dependent dielectric constant and nonlinear susceptibility in $SrTiO_3$, Phys. Rev. B **52**, 13159 (1995).

[36] H. B. Zhang and M. Alexe, Optoelectronic functionality of $BiFeO_3$-$SrTiO_3$ interface, Adv. Electron. Mater. **8**, 2100665 (2022).

[37] P. Noel, F. Trier, L. V. M. Arche, J. Brehin, D. C. Vaz, V. Garcia, S. Fusil, A. Barthelemy, L. Vila, M. Bibes, *et al.*, Non-volatile electric control of spin-charge conversion in a $SrTiO_3$ Rashba system, Nature **580**, 483 (2020).

[38] Y. Heo, H. B. Zhang, and M. Alexe, Dynamic control of piezoelectricity enhancement via modulation of the bulk photovoltaic effect in a $BiFeO_3$ thin film. Adv. Electron. Mater. **8** (2022).